Atmospheric and Oceanic Science Letters

ISSN: 1674-2834 (Print) 2376-6123 (Online) Journal homepage: http://www.tandfonline.com/loi/taos20

Cloud microphysical differences with precipitation intensity in a torrential rainfall event in Sichuan, China

Yong-Jie Huang, Xiao-Peng Cui & Ya-Ping Wang

To cite this article: Yong-Jie Huang, Xiao-Peng Cui & Ya-Ping Wang (2016) Cloud microphysical differences with precipitation intensity in a torrential rainfall event in Sichuan, China, Atmospheric and Oceanic Science Letters, 9:2, 90-98

To link to this article: http://dx.doi.org/10.1080/16742834.2016.1139436

Published online: 23 Feb 2016.

ATMOSPHERIC AND OCEANIC SCIENCE LETTERS, 2016
VOL. 9, NO. 2, 90–98
http://dx.doi.org/10.1080/16742834.2016.1139436

Taylor & Francis
Taylor & Francis Group

Cloud microphysical differences with precipitation intensity in a torrential rainfall event in Sichuan, China

HUANG Yong-Jie[a,b], CUI Xiao-Peng[a,c] and WANG Ya-Ping[a,b]

[a]Key Laboratory of Cloud-Precipitation Physics and Severe Storms, Institute of Atmospheric Physics, Chinese Academy of Sciences, Beijing 100029, China; [b]College of Earth Science, University of Chinese Academy of Sciences, Beijing 100049, China; [c]Collaborative Innovation Center on Forecast and Evaluation of Meteorological Disasters, Nanjing University of Information Science & Technology, Nanjing 210044, China

ABSTRACT

High-resolution data of a torrential rainfall event in Sichuan, China, simulated by the WRF model, were used to analyze the cloud microphysical differences with precipitation intensity. Six-hourly accumulated rainfall was classified into five bins based on rainfall intensity, and the cloud microphysical characteristics and processes in different bins were studied. The results show that: (1) Hydrometeor content differed distinctly among different bins. Mixing ratios of cloud water, rain water, and graupel enhanced significantly and monotonously with increasing rainfall intensity. With increasing precipitation intensity, the monotonous increase in cloud water number concentration was significant. Meanwhile, number concentrations of rain water and graupel increased at first and then decreased or increased slowly in larger rainfall bins. (2) With precipitation intensity increasing, cloud microphysical conversion processes closely related to the production of rainwater, directly (accretion of cloud water by rain (QCL_{cr}) and melting of graupel (QML_{gr})) or indirectly (water vapor condensation and accretion of cloud water by graupel), increased significantly. (3) As the two main sources of rainwater, QCL_{cr} increased monotonously with increasing precipitation intensity, while QML_{gr} increased slowly, even tending to cease increasing in larger rainfall bins.

摘要

降水是由复杂的动力、热力和云微物理过程相互作用产生。为了揭示四川暴雨过程的云微物理特征，利用WRF模式对四川一次暴雨过程的高分辨率模拟资料，研究不同强度降水中云微物理特征和过程的差异。结果显示，水凝物含量在不同强度降水中显著不同；随着降水强度增强，与雨水产生直接或间接相关的云微物理转化过程明显增强；作为雨水的两个主要源项，云水被雨水碰并收集（QCL_{cr}）随着降水强度增强而单调递增，而霰融化（QML_{gr}）增长较为缓慢。

ARTICLE HISTORY
Received 26 July 2015
Revised 12 November 2015
Accepted 18 December 2015

KEYWORDS
Cloud microphysics; cloud microphysical processes; torrential rainfall; numerical simulation

1. Introduction

Torrential rainfall can cause floods, debris flows, and other natural disasters. In Sichuan Province, China, where the terrain is complex, heavy rainfall is more likely to cause floods and other disasters. Thus, accurate forecasting of rainstorms in this region is very important. During the past 20 years, the development of high-resolution mesoscale numerical models, such as MM5 and the WRF model, have led to improved understanding and prediction of local weather, especially precipitation. However, precipitation is produced from the interaction among complex dynamic, thermodynamic, and cloud microphysical processes. Thus, accurate quantitative precipitation forecasts remain a huge challenge to researchers and forecasters. Over the past few decades, the dynamic and thermodynamic processes affecting precipitation have become well understood (Neiman et al. 2002; Jiang 2003; Mapes, Warner, and Xu 2003; Galewsky and Sobel 2005; Medina et al. 2005; Garvert, Smull, and Mass 2007; Colle, Smith, and Wesley 2013; Siler and Roe 2014), but the mechanisms of cloud microphysical processes in precipitation cloud lack an in-depth and comprehensive understanding, meaning more detailed and comprehensive studies on cloud microphysical processes and budgets associated with heavy rainfall are required (Colle and Zeng 2004a, 2004b; Colle et al. 2005).

Li, Cui, and Cao (2014) conducted a high-resolution numerical simulation of a torrential rainfall event in Sichuan using the WRF model and discussed the effects of large-scale circulation and mesoscale systems on the rainstorm against the background of complex terrain. Huang and Cui (2015) further studied the dominant cloud microphysical processes of this torrential rainfall event using the same model setup. They found that raindrops

CONTACT CUI Xiao-Peng xpcui@mail.iap.ac.cn

were mainly generated via two paths: in the first, water vapor condensed into cloud water, the accretion of cloud water by graupel formed graupel, and then the melting of graupel formed rain water; while in the second, water vapor condensed into cloud water, and the accretion of cloud water by rain water formed rain water. Cui, Wang, and Yu (2015) studied the cloud microphysical differences among various rainfall intensities for severe tropical storm Bilis (2006), and found that the magnitude of accretion of cloud water by rain monotonously increased with increasing precipitation intensity, while the magnitude of graupel melting increased at first and then decreased. As an extension of that work, the present study asks: are there similar characteristics for torrential rainfall in Sichuan, against the background of complex terrain? To answer this question, cloud microphysical differences with precipitation intensity during a torrential rainfall event were analyzed using the same simulation data as Huang and Cui (2015).

2. Model and methodology

Huang and Cui (2015) used the WRF model to simulate a torrential rainfall event in Sichuan, China, which occurred from 1800 UTC 17 August to 0000 UTC 20 August 2010. The simulation was integrated for 54 h, using three domains with horizontal resolutions of 27, 9, and 3 km. In the 3-km resolution domain, a cumulus convective parameterization scheme was not used (for details of the model setup and verification, see Li, Cui, and Cao (2014) and Huang and Cui (2015)). The cloud microphysical scheme used in Huang and Cui (2015) was the Milbrandt 2-mom scheme (Milbrandt and Yau 2005a, 2005b), which takes seven kinds of water species into consideration: water vapor (Q_{vapor}), cloud water (Q_c), rain water (Q_r), cloud ice (Q_i), snow (Q_s), graupel (Q_g), and hail (Q_h). Detail regarding the microphysical conversion processes can be found in Milbrandt and Yau (2005b) and the Appendix of the present paper. This study focused on two heavy rainfall periods in the (28–33°N, 100–106°E) region of the 3-km resolution domain: 1800 UTC 18 August to 0000 UTC 19 August 2010, and 0000 to 0600 UTC 19 August 2010. The main reason for selected these two periods was to illustrate whether the results obtained in this study are similar in different rainfall periods. Figure 1 shows observed and simulated radar reflectivity and simulated 6-h accumulated precipitation in the two precipitation periods. The locations of the strong radar echo bands in the simulation are close to those observed (Figures 1a–1d). Due to the radar detection range and the Tibetan Plateau, the observed radar echo covers a smaller range. Heavy rainfall bands orient southwest–northeast in both periods and the distribution of precipitation in the second period is narrower. A number of strong rainfall centers scatter throughout the rainfall belts in both periods.

Based on the precipitation grading standards used at the National Meteorological Center, China, the 6-h accumulated precipitation amounts (P6 for short) were classified into five bins based on rainfall intensity: 0.1–13, 13–25, 25–60, 60–120 mm, and larger than 120 mm. Table 1 shows the grid numbers and mean 6-h accumulated rainfall of each bin. The grid-mean precipitation in the bins of 0.1–13, 13–25, 25–60, and 60–120 mm are similar between the two periods. Meanwhile, the grid numbers in the second period are much less than those in the first period in the bins of 25–60, 60–120 mm, and larger than 120 mm, indicating the precipitation system gradually weakened in the second period (Figure 1).

3. Cloud microphysical differences

3.1 Mixing ratio, number concentration, and mean mass diameter

Figure 2 shows the variations of spatiotemporally averaged water species' mixing ratios (Figures 2a and 2b), number concentrations (Figures 2c and 2d) and mean mass diameters (Figures 2e and 2f) with rainfall intensity. The mixing ratios of hydrometeors showed distinct differences among different intensities of precipitation, and the hail mixing ratio (Q_h) was negligibly small during this event. Although there were some differences between the two periods, similar features existed. The mixing ratios of cloud water (Q_c), rain water (Q_r), and graupel (Q_g) significantly and monotonously increased with increasing rainfall intensity. These features were closely related to the macro dynamic fields. From the vertical velocity profiles in various precipitation bins in the two precipitation periods (Figure 3), vertical velocities substantially increased with increasing precipitation intensity. In the second period, the mixing ratio of solid hydrometeors (the sum of the mixing ratios of cloud ice, snow, and graupel) was much smaller than that in the first period, associated with much weaker updraft velocities above the zero-layer in the second period compared with those in the first period (Figure 3). In the first period, the mixing ratio of solid hydrometeors was larger than that of liquid hydrometeors (the sum of the mixing ratios of cloud water and rainwater) in the first three rainfall bins, and smaller than that of liquid hydrometeors in the largest rainfall bin. This may have been related to the much stronger upward motion above the zero-layer, especially from 9 to 16 km in the largest rainfall bin (Figure 3a). In the second period, the mixing ratio of solid hydrometeors was a little larger than that of liquid hydrometeors in the smallest rainfall bin, but much smaller than that of liquid hydrometeors in larger rainfall bins. This

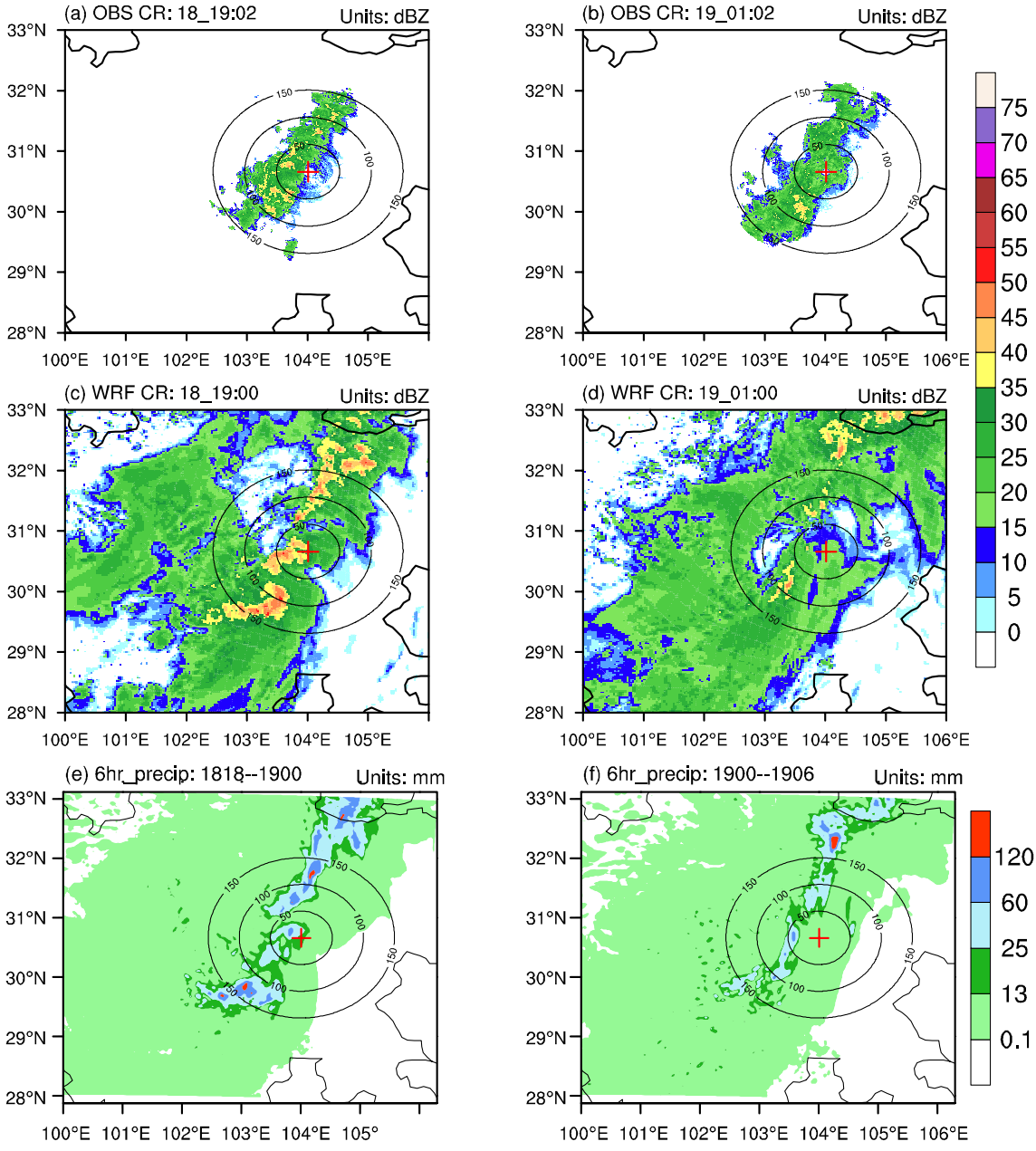

Figure 1. (a, b) Observed and (c, d) simulated radar composite reflectivity (shaded; units: dBZ). The times for (a) and (c) are 1902 and 1900 UTC 18 August 2010, respectively. The times for (b) and (d) are 0102 and 0100 UTC 19 August 2010, respectively. Distributions of 6-h accumulated precipitation (shaded; units: mm) in the (28–33°N, 100–106°E) region of the 3-km resolution domain: (e) 1800 UTC 18 August to 0000 UTC 19 August 2010; (f) 0000 to 0600 UTC 19 August 2010. The red ' + ' represents Chengdu radar station. Black contours represent the distance from Chengdu radar station.

Table 1. Grid number and mean six-hourly accumulated precipitation (P6) of each precipitation bin in the (28–33°N, 100–106°E) region of the 3-km resolution domain.

Precipitation (mm) bin	0.1 ≤ P6 < 13		13 ≤ P6 < 25		25 ≤ P6 < 60		60 ≤ P6 < 120		120 ≤ P6	
Period	GN[a]	MP[b]	GN	MP	GN	MP	GN	MP	GN	MP
1818–1900	24,159	3.4	1,579	18.2	1,537	37.7	438	80.8	33	133.6
1900–06	24,520	3.3	1,433	17.7	993	37.2	105	74.9	21	161.4

[a]Grid number.
[b]Mean precipitation (units: mm).

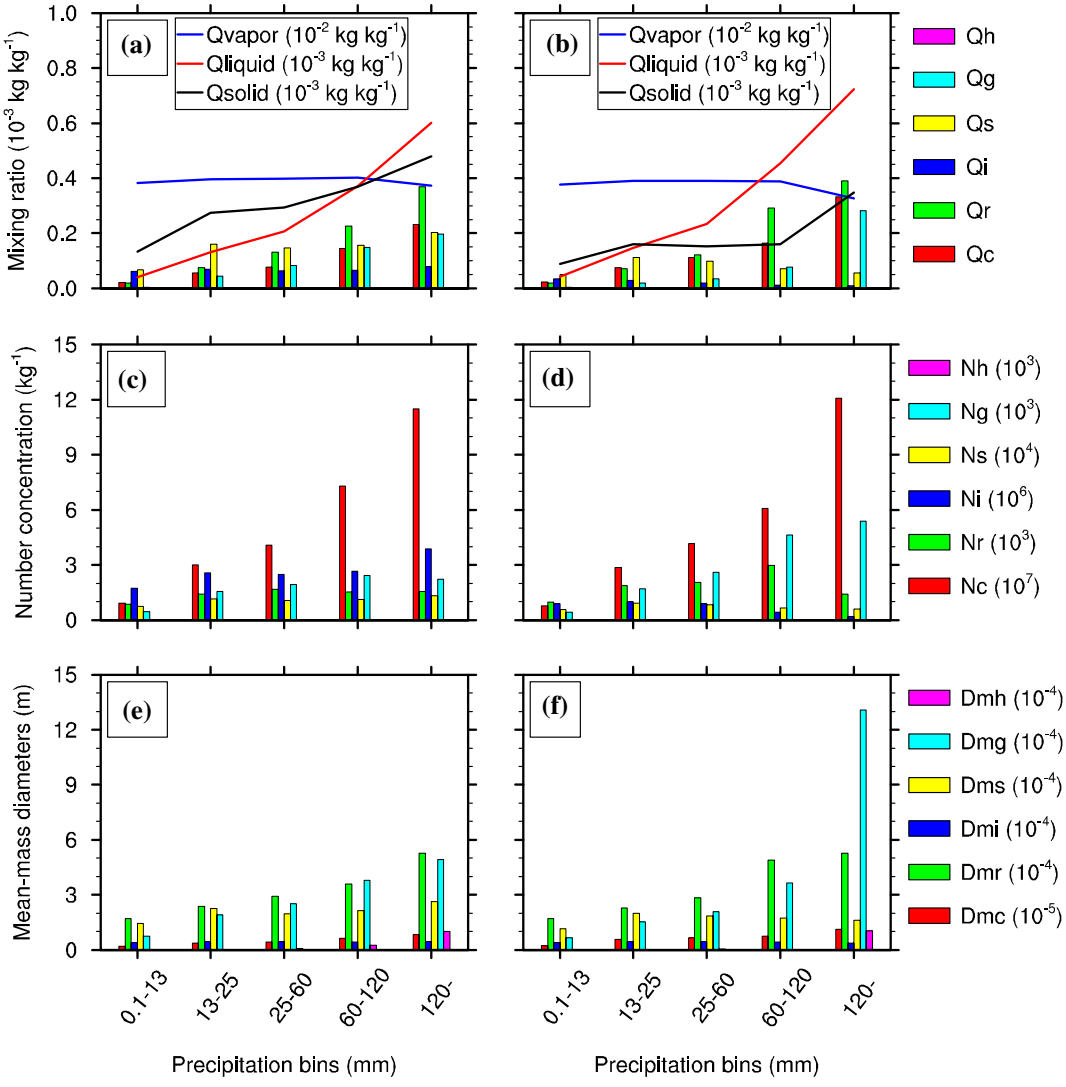

Figure 2. (a, b) Variations of water species' mixing ratios, (c, d) number concentrations, and (e, f) mean-mass diameters with increasing precipitation intensity during 1800 UTC 18 August to 0000 UTC 19 August 2010 (left column) and 0000 to 0600 UTC 19 August 2010 (right column). Their units are shown in the figures. In (a) and (b), blue curves represent water vapor mixing ratios, red curves represent liquid hydrometeor mixing ratios, and black curves represent solid hydrometeor mixing ratios.

resulted from the fact that the vertical velocity in the second period mainly concentrated in the lower troposphere around the zero-layer. Overall, the above discussion shows that both solid and liquid hydrometeors dominated in the first period, while liquid hydrometeors played a greater role in the second period. It should be noted that, in the second period, from the bin of 60–120 mm to the bin of P6 ≥ 120 mm, the mixing ratio of graupel increased sharply and contributed to the sharp overall increase for solid hydrometeors. This implies that, although liquid hydrometeors dominated overall in the second period, graupel concentrated in the largest rainfall bin and contributed to the surface rainfall there. From Huang and Cui (2015), graupel mainly distributed near the zero-layer; and from the present results (Figure 3b), updraft velocities near the zero-layer reached their maximum in the largest rainfall bin in the second precipitation period. Therefore, the probability of collision between graupel and cloud droplets, and graupel and raindrops, increased, and the mixing ratio and diameter of graupel increased significantly (Figures 2b and 2f). It should also be noted that, in the first period (Figure 2a), the mixing ratios of snow and cloud ice were larger than those in the second period. However, since they contributed little to surface rainfall (Huang and Cui 2015), this aspect is discussed no further here. Additionally, their roles mainly involved helping to increase the overall solid hydrometeor mixing ratio in this period. Meanwhile, the water vapor supply and its variation with rainfall intensity was similar in the two periods (Q_{vapor}; blue curves in Figures 2a and 2b, both greater than 0.35×10^{-2} kg kg^{-1}, which provided ample moisture for the heavy rainfall in the two periods.

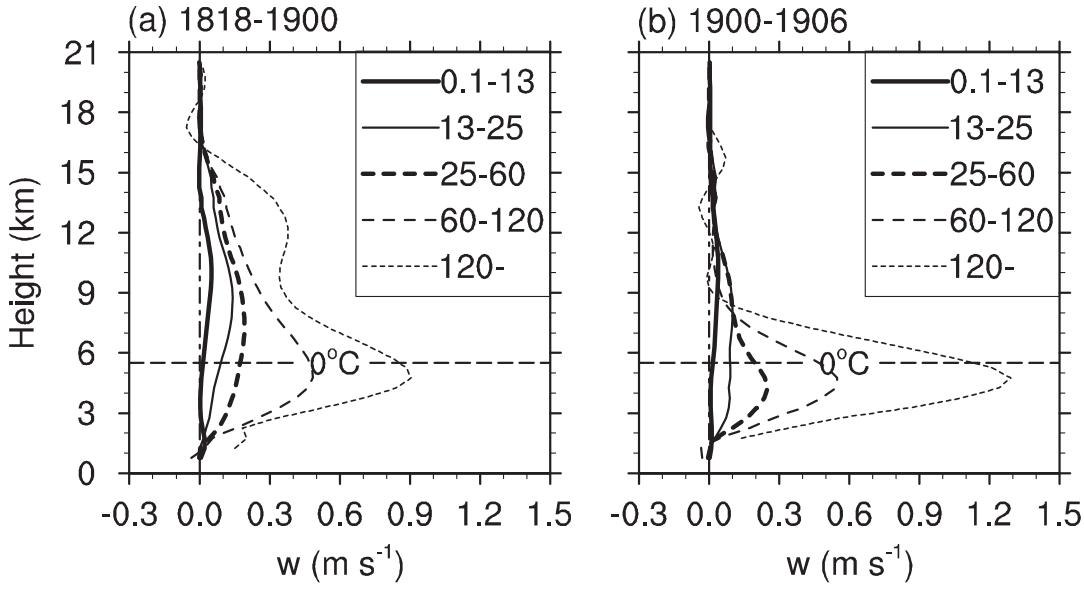

Figure 3. Vertical velocity profiles in various precipitation bins (units: m s^{-1}). The horizontal dashed lines represent averaged zero-layer height of all precipitation grids: (a) 1800 UTC 18 August to 0000 UTC 19 August 2010; (b) 0000 UTC to 0600 UTC 19 August 2010.

In Figures 2c and 2d, with increasing precipitation intensity, the change in cloud water number concentration (N_c) was significant, increasing from about 1×10^7 kg^{-1} in the 0.1–13 mm bin to about 11.6×10^7 kg^{-1} in the P6 ≥ 120 mm bin in the first period, and from approximately 0.8×10^7 kg^{-1} in the 0.1–13 mm bin to approximately 12×10^7 kg^{-1} in the P6 ≥ 120 mm bin in the second period. The rain water number concentration (N_r) increased at first and then decreased with increasing precipitation intensity in both periods, indicating that raindrops became dense, and collisions with each other resulted in larger raindrops in heavy rainfall (Figures 2c–2f). The graupel number concentration (N_g) also increased at first and then decreased with increasing precipitation intensity in the first period, but increased at first and then lowered its rate of increase in the P6 ≥ 120 mm rainfall bin in the second period. In the second period, N_g was much larger than that in the first period, especially in larger rainfall bins. This may have been related to the much stronger upward motion in the P6 ≥ 120 mm rainfall bin in the second period than that in the first period (Figure 3).

From Figures 2e and 2f, the mean-mass diameters of cloud water and cloud ice possessed smaller magnitudes, and those of the other three hydrometeors (rainwater, snow, and graupel) possessed larger magnitudes, identical to their physical natures. The mean-mass diameters of rainwater, snow, and graupel were similar, except in stronger rainfall bins where the mean-mass diameters of rainwater and graupel were more similar and both larger than that of snow. It is noted that, in the second period, the mean-mass diameter of graupel increased sharply from the bin of 60–120 mm to the bin of P6 ≥ 120 mm, similar to the variation in the mixing ratio of graupel (Figure 2b). This implies that, although overall the liquid hydrometeors dominated in the second period, graupel dominated (or concentrated) in the largest rainfall bin (P6 ≥ 120 mm) with a larger mixing ratio and mean-mass diameter due to the strong upward motion near the zero-layer, which increased the probability of collision between graupel and cloud droplets, and graupel and raindrops (Figure 3b).

Overall, the cloud microphysical characteristics were closely related to large-scale dynamics. Due to different distributions of vertical motion, the development of solid hydrometeor particles and ice-phase processes was more vigorous in the first period, while the growth of liquid hydrometeors and warm cloud processes may have been the key features in the second period.

3.2 Cloud microphysical conversion processes

Figure 4 shows the main cloud microphysical conversion processes of water vapor (Figures 4a and 4b), cloud water (Figures 4c and 4d), rain water (Figures 4e) and 4f), cloud ice (Figures 4g and 4h), snow (Figures 4i and 4j), and graupel (Figures 4k and 4l) in various precipitation bins during 1800 UTC 18 August to 0000 UTC 19 August 2010, and 0000 to 0600 UTC 19 August 2010. For the same types of water species, the main source and sink terms in the budgets of the species were similar among different precipitation bins in both periods. For example, in the budget of water vapor, water vapor condensation (QVD_{vc}) was the main sink term in both periods. Furthermore, the accretion of cloud water by rain to form rain (QCL_{cr}) and the melting of graupel to rain (QML_{gr}) were the two main source terms for

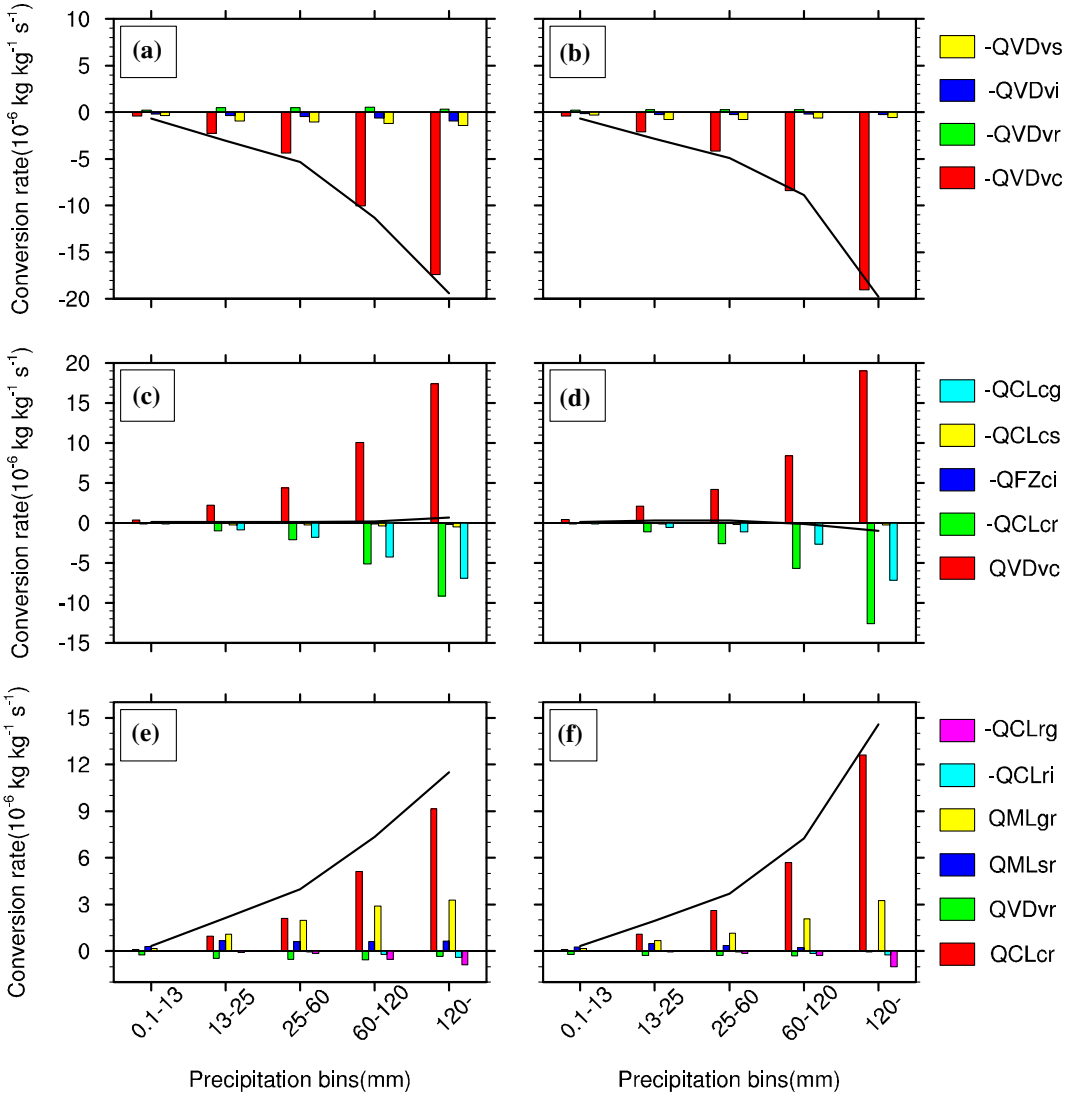

Figure 4. Variation in the major cloud microphysical conversion rates with precipitation intensity during 1800 UTC 18 August to 0000 UTC 19 August 2010 (left column) and 0000 to 0600 UTC 19 August 2010 (right column): (a, b) water vapor; (c, d) cloud water; (e, f) rain water; (g, h) cloud ice; (i, j) snow; (k, l) graupel. Black curves represent the sum of each water species' source and sink terms. Units are 10^{-6} kg kg^{-1} s^{-1}.

the production of rainwater. These results are consistent with the findings of Huang and Cui (2015).

With increasing precipitation intensity, almost all the major cloud microphysical conversion processes, especially those processes closely related to the production of rainwater and surface rainfall, directly (QCL_{cr} and QML_{gr}) or indirectly (QVD_{vc} and accretion of cloud water by graupel to form graupel (QCL_{cg})), increased significantly. The net growth rates of cloud ice and snow in the first period increased with precipitation intensity (Figures 4g and 4i), while they changed little, and even reduced, in the second period (Figures 4h and 4j). Meanwhile, they were smaller in the second period than those in the first period. Additionally, it was closely related to the different distributions of updraft velocities (Figure 3) and solid hydrometeors between the two periods (Figures 2a and 2b). Meanwhile, the magnitudes of ice- and snow-related microphysical conversion processes were significantly smaller than those related to cloud water, rain water, and graupel. Therefore, ice-phase microphysics did not play a dominant role in this precipitation process.

Water vapor condensation (QVD_{vc}) was the main sink term in the water vapor budget (Figures 4a and 4b), and increased significantly as precipitation intensity enhanced. Abundant water vapor is transported to the rainstorm region and feeds the development of cloud systems and surface rainfall. Cloud water with QVD_{vc} as its main source was mainly consumed by QCL_{cr} and QCL_{cg} to form rainwater and graupel, respectively (Figures 4c and 4d). QVD_{vc} and QCL_{cr} in the bin of P6 ≥ 120 mm in the second period were larger than those in the first period. The vertical

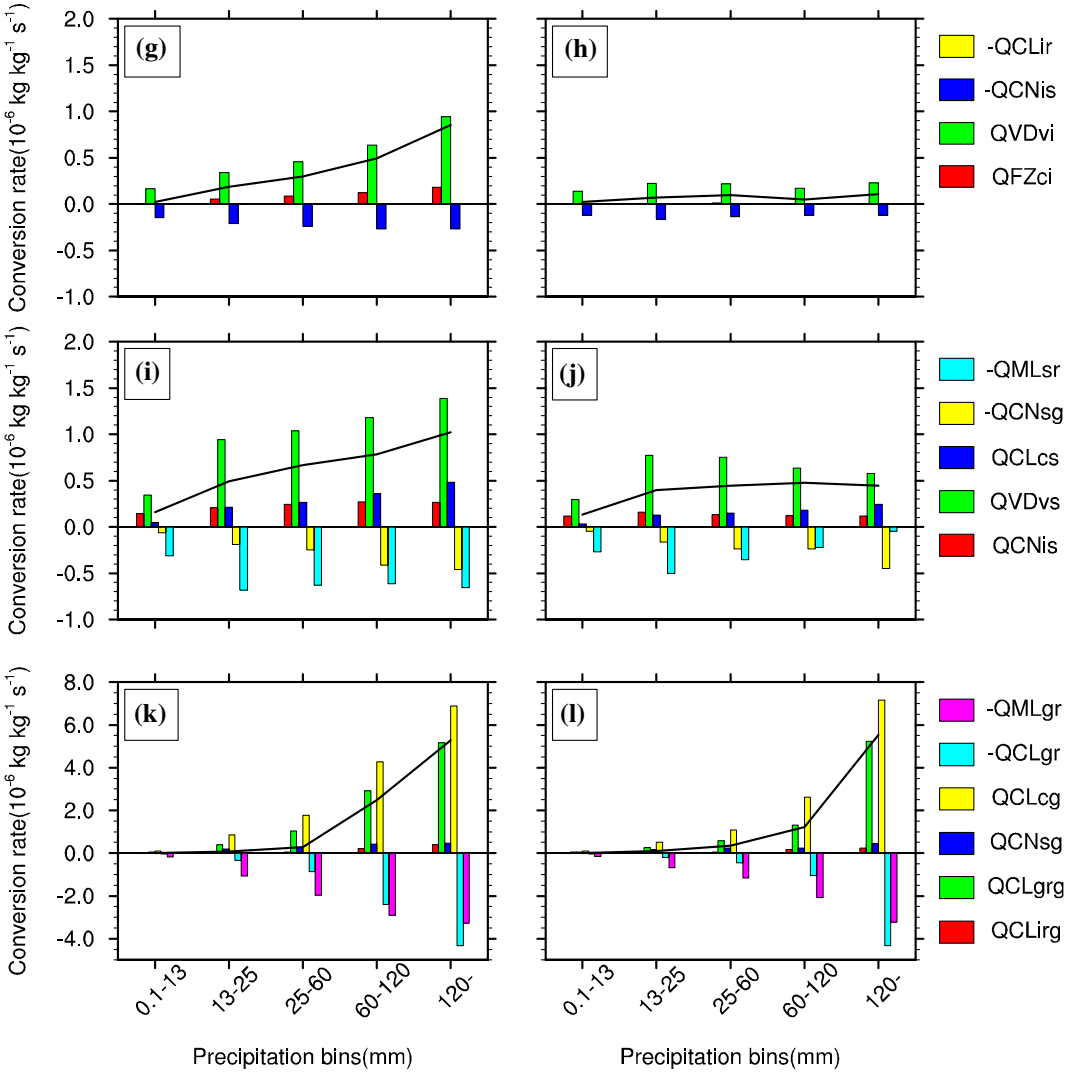

Figure 4. (*Continued*)

velocity below the zero-layer in the bin of P6 ≥ 120 mm in the second period was stronger than that of the first period (Figures 3a and 3b), which may have enhanced the condensation of water vapor and the accretion of cloud water by rain. As the two main sources of rainwater (Figures 4e and 4f), QCL_{cr} increased monotonously with increasing precipitation intensity, while QML_{gr} increased slowly, and even tended to cease increasing or decrease (Figure 4e). These characteristics are similar to those reported for severe tropical storm Bilis (Cui, Wang, and Yu, 2015).

Compared with the weaker conversion rates associated with cloud ice and snow (Figures 4g–4j), the conversion processes related to graupel were the most important ice-phase processes (Figures 4k and 4l); plus, QCL_{cg} was the main source term and QML_{gr} was the main sink term in the budget of graupel. With increasing rainfall intensity, QCL_{cg} and QML_{gr} increased accordingly in both periods. Besides, the source term of graupel, i.e. collision between graupel and rainwater to form graupel (QCL_{grg}), consumed graupel (QCL_{gr}), and rain water (QCL_{rg}) simultaneously. Since the absolute values of QCL_{grg} and QCL_{gr} were similar in all precipitation bins, the net growth of graupel by graupel–rain collision and coalescence (QCL_{grg}–QCL_{gr}) was small, indicating that it was not a major source or sink term for graupel (Figures 4k and 4l).

4. Summary

By using high-resolution numerical simulation data of a torrential rainfall event in Sichuan, China, two 6-h accumulated rainfalls were classified into five bins based on rainfall intensity, and the cloud microphysical variation with precipitation intensity during the torrential rainfall event was studied. The major findings can be summarized as follows:

(1) The mixing ratios of water species showed distinct differences among different intensities of precipitation. The water vapor supply and its

variation with rainfall intensity was similar in the two periods, providing ample moisture for the heavy rainfall. Cloud water (Q_c), rain water (Q_r), and graupel (Q_g) significantly and monotonously increased with increasing rainfall intensity in both periods. In the second period, the mixing ratio of solid hydrometeors was much smaller than that in the first period. Both solid and liquid hydrometeors dominated in the first period, while liquid hydrometeors dominated in the second period. Moreover, in the second period, graupel dominated (or concentrated) in the largest rainfall bin, with larger mixing ratios and mean-mass diameters, and contributed to the surface rainfall there.

(2) The cloud water number concentration (N_c) increased significantly with increasing precipitation intensity. However, the rain water number concentration (N_r) increased at first and then decreased with increasing precipitation intensity in both periods. The graupel number concentration (N_g) also increased at first and then decreased with increasing precipitation intensity in the first period, but increased at first and then lowered its rate of increase in the largest rainfall bin in the second period.

(3) With increasing precipitation intensity, almost all the major cloud microphysical conversion processes in the budgets, especially those processes closely related to the production of rainwater and surface rainfall, directly (QCL_{cr} and QML_{gr}) or indirectly (QVD_{vc} and QCL_{cg}), increased significantly. In this case, cloud ice and snow contributed little to the surface rainfall and may have mainly contributed to the development of the cloud systems. Water vapor condensation (QVD_{vc}), the main sink in the water vapor budget, increased significantly with the enhanced precipitation intensity. Cloud water, whose main source was from QVD_{vc}, was mainly consumed by QCL_{cr} and QCL_{cg} to form rainwater and graupel, respectively. As the two main sources of rainwater, QCL_{cr} increased monotonously with increasing precipitation intensity, while QML_{gr} increased slowly, and even tended to cease increasing. These results are similar to those reported for severe tropical storm Bilis (Cui, Wang, and Yu, 2015).

The cloud microphysical variation with precipitation intensity shown in this study was closely related to the distribution of the large-scale vertical motion. Therefore, the combination of large-scale dynamics and cloud microphysics is very important when studying rainfall events. Finally, it is important to note that caution should be exercised in terms of the applicability of the present results, since only one event was analyzed. It is necessary to examine multiple torrential rainfall events to validate the results of this study.

Acknowledgements

The authors thank the three anonymous reviewers for their helpful comments on the manuscript.

Funding

This work was supported by the Key Research Program of the Chinese Academy of Sciences [grant number KZZD-EW-05-01] and the National Basic Research Program of China [973 Program, grant number 2014CB441402]. This work was carried out at the National Supercomputer Center in Tianjin, and the calculations were performed on TianHe-1(A).

Notes on contributors

HUANG Yong-Jie is a PhD candidate at the Institute of Atmospheric Physics (IAP), Chinese Academy of Sciences (CAS). His main research interests are numerical modeling, cloud microphysics, and severe convective systems. His recent publications include papers in Journal of Hydrometeorology, Atmospheric Research, Advances in Atmospheric Sciences, Atmospheric Science Letters, and other journals.

CUI Xiao-Peng is a professor at IAP, CAS. His main research interests are tropical cyclone, heavy rainfall, dynamics and numerical simulation, surface rainfall processes. His recent publications include papers in Journal of Hydrometeorology, Journal of Geophysical Research-Atmospheres, Atmospheric Research, Science China: Earth Sciences, Advances in Atmospheric Sciences, Atmospheric Science Letters, and other journals.

WANG Ya-Ping is also a PhD candidate at IAP, CAS. Her main research interests are tropical cyclone simulation and diagnosis. Her recent publications include papers in Atmospheric Science Letters and Chinese Journal of Atmospheric Sciences.

References

Colle, B. A., and Y. G. Zeng. 2004a. "Bulk Microphysical Sensitivities within the MM5 for Orographic Precipitation. Part I: The Sierra 1986 Event." *Monthly Weather Review* 132 (12): 2780–2801.

Colle, B. A., and Y. G. Zeng. 2004b. "Bulk Microphysical Sensitivities within the MM5 for Orographic Precipitation. Part II: Impact of Barrier Width and Freezing Level." *Monthly Weather Review* 132 (12): 2802–2815.

Colle, B. A., M. F. Garvert, J. B. Wolfe, C. F. Mass, and C. P. Woods. 2005. "The 13–14 December 2001 IMPROVE-2 Event. Part III: Simulated Microphysical Budgets and Sensitivity Studies." *Journal of the Atmospheric Sciences* 62 (10): 3535–3558.

Colle, B. A., R. B. Smith, and D. A. Wesley. 2013. "Theory, Observations, and Predictions of Orographic Precipitation" In *Mountain Weather Research and Forecasting: Recent Progress and Current Challenges*, edited by Fotini K. Chow, Stephan F.J. De Wekker, and Bradley J. Snyder, 291–344. Heidelberg: Springer.

Cui, X. P., Y. P. Wang, and H. Yu. 2015. "Microphysical Differences with Rainfall Intensity in Severe Tropical Storm Bilis." *Atmospheric Science Letters* 16 (1): 27–31.
Galewsky, J., and A. Sobel. 2005. "Moist Dynamics and Orographic Precipitation in Northern and Central California during the New Year's Flood of 1997." *Monthly Weather Review* 133 (6): 1594–1612.
Garvert, M. F., B. Smull, and C. Mass. 2007. "Multiscale Mountain Waves Influencing a Major Orographic Precipitation Event." *Journal of the Atmospheric Sciences* 64 (3): 711–737.
Huang, Y. J., and X. P. Cui. 2015. "Dominant Cloud Microphysical Processes of a Torrential Rainfall Event in Sichuan, China." *Advances in Atmospheric Sciences* 32 (3): 389–400.
Jiang, Q. F. 2003. "Moist Dynamics and Orographic Precipitation." *Tellus A* 55 (4): 301–316.
Li, Q., X. P. Cui, and J. Cao. 2014. "The Observational Analysis and Numerical Simulation of a Heavy Rain Event in Sichuan Province." *Chinese Journal of Atmospheric Sciences* 38 (6): 1095–1108. doi: 10.3878/j.issn.1006-9895.1401.13255 (in Chinese).
Mapes, B. E., T. T. Warner, and M. Xu. 2003. "Diurnal Patterns of Rainfall in Northwestern South America. Part III: Diurnal Gravity Waves and Nocturnal Convection Offshore." *Monthly Weather Review* 131 (5): 830–844.
Medina, S., B. F. Smull, R. A. Houze, and M. Steiner. 2005. "Cross-barrier Flow during Orographic Precipitation Events: Results from MAP and IMPROVE." *Journal of the Atmospheric Sciences* 62 (10): 3580–3598.
Milbrandt, J. A., and M. K. Yau. 2005a. "A Multimoment Bulk Microphysics Parameterization. Part I: Analysis of the Role of the Spectral Shape Parameter." *Journal of the Atmospheric Sciences* 62 (9): 3051–3064.
Milbrandt, J. A., and M. K. Yau. 2005b. "A Multimoment Bulk Microphysics Parameterization. Part II: A Proposed Three-moment Closure and Scheme Description." *Journal of the Atmospheric Sciences* 62 (9): 3065–3081.
Neiman, P. J., F. M. Ralph, A. B. White, D. E. Kingsmill, and P. O. G. Persson. 2002. "The Statistical Relationship between Upslope Flow and Rainfall in California's Coastal Mountains: Observations during CALJET." *Monthly Weather Review* 130 (6): 1468–1492.
Siler, N., and G. Roe. 2014. "How Will Orographic Precipitation Respond to Surface Warming? An Idealized Thermodynamic Perspective." *Geophysical Research Letters* 41 (7): 2606–2613.

Appendix

This appendix presents the detailed microphysical conversion processes of the cloud microphysical scheme; namely, the Milbrandt 2-mom scheme (Milbrandt and Yau 2005a, 2005b). The tendencies for the mixing ratios are

$$S_{Q_v} = -QVD_{vc} - QVD_{vr} - QNU_{vi} - QVD_{vi} - QVD_{vs} - QVD_{vg} - QVD_{vh}, \quad (1)$$

$$S_{Q_c} = QVD_{vc} - QCN_{cr} - QCL_{cr} - QFZ_{ci} - QCL_{ci} - QCL_{cs} - QCL_{cg} - QCL_{ch}, \quad (2)$$

$$S_{Q_r} = QCN_{cr} + QCL_{cr} + QVD_{vr} + QML_{ir} + QML_{sr} + QML_{gr} + QML_{hr} - QCL_{ri} - QCL_{rs} - QCL_{rg} - QCL_{rh} - QFZ_{rh}, \quad (3)$$

$$S_{Q_i} = QNU_{vi} + QFZ_{ci} + QVD_{vi} + QIM_{si} + QIM_{gi} + QCL_{ci} - QCL_{ir} - QCL_{is} - QCL_{ig} - QCL_{ih} - QCN_{is} - QCN_{ig} - QML_{ir}, \quad (4)$$

$$S_{Q_s} = \delta_{srs}(QCL_{rs} + QCL_{sr}) + QCN_{is} + QVD_{vs} + QCL_{cs} + QCL_{is} - QCN_{sg} - QCL_{sr} - QCL_{sh} - QIM_{si} - QML_{sr}, \quad (5)$$

$$S_{Q_g} = \delta_{irg}(QCL_{ir} + QCL_{ri}) + \delta_{srg}(QCL_{sr} + QCL_{rs}) + \delta_{grg}(QCL_{gr} + QCL_{rg}) + QCN_{ig} + QCN_{sg} + QCL_{cg} + QCL_{ig} - QCL_{gr} + QVD_{vg} - QCN_{gh} - QML_{gr} - QIM_{gi} \quad (6)$$

$$S_{Q_h} = \delta_{irh}(QCL_{ir} + QCL_{ri}) + \delta_{srh}(QCL_{sr} + QCL_{rs}) + \delta_{grh}(QCL_{gr} + QCL_{rg}) + QFZ_{rh} + QCN_{gh} + QCL_{ch} + QCL_{rh} + QCL_{ih} + QCL_{sh} + QVD_{vh} - QML_{hr}, \quad (7)$$

where, S_{Q_v}, S_{Q_c}, S_{Q_r}, S_{Q_i}, S_{Q_s}, S_{Q_g}, and S_{Q_h} are the microphysical source/sink terms of water vapor and cloud species, respectively. The notation for the terms involving two interacting categories is denoted by QAB_{yx}, where Q is the mass mixing ratio of the prognostic variable, AB represents microphysical processes (VD for diffusional growth, NU for nucleation, CN for conversion, CL for collection, FZ for freezing, ML for melting, and IM for ice multiplication), and the subscript 'yx' indicates that mass is being transferred from category y to x ($x, y \in (v, c, r, i, s, g, h)$ denote various water species). δ_{xry} is a determination coefficient meaning that category x (s, i, g) and rain water collide to form category y (s, g, h). For example, if rain water and snow collide to form graupel, then $\delta_{srg} = 1, \delta_{srs} = 0$, and $\delta_{srh} = 0$ (also see Milbrandt and Yau (2005b)).